Applied Surface Science 554 (2021) 149656

Contents lists available at ScienceDirect

Applied Surface Science

journal homepage: www.elsevier.com/locate/apsusc

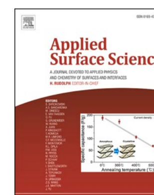

Full Length Article

Tris(dimethylamido)aluminum(III) and N_2H_4: Ideal precursors for the low-temperature deposition of large grain, oriented c-axis AlN on Si via atomic layer annealing

Scott T. Ueda [a], Aaron McLeod [b], Dan Alvarez [c], Daniel Moser [d], Ravindra Kanjolia [d], Mansour Moinpour [d], Jacob Woodruff [d], Andrew C. Kummel [b,*]

[a] *Materials Science and Engineering Program, University of California, San Diego, La Jolla, CA 92093, USA*
[b] *Department of Chemistry and Biochemistry, University of California, San Diego, La Jolla, CA 92093, USA*
[c] *Rasirc, Inc, San Diego, CA 92126, USA*
[d] *EMD Performance Materials, Haverhill, MA 01832, USA*

ARTICLE INFO

Keywords:
AlN
Back end of line (BEOL)
Atomic layer annealing (ALA)
Low-temperature
X-ray photoelectron spectroscopy (XPS)
Plasma

ABSTRACT

The low-temperature (≤400 °C) deposition of polycrystalline AlN films on silicon is demonstrated by atomic layer annealing (ALA) using either trimethyl aluminum (TMA) and anhydrous hydrazine (N_2H_4) or tris(dimethylamido) aluminum (TDMAA) and anhydrous N_2H_4 with an argon plasma treatment utilizing a DC bias to tune the ion energy. Using TDMAA and N_2H_4, high-quality AlN films are deposited with large grain size and low oxygen/carbon contamination which can be used as a templating layer for further high-speed AlN film growth via sputtering. The deposition of high-quality AlN films deposited by ALA are successfully used as templates for sputtered AlN resulting in a >2x improvement in average grain size when compared to an analogous amorphous template layer.

1. Introduction

High-quality, large-grained AlN films are of interest for use in a number of applications such as for heat spreading layers [1–3] or as a buffer/templating layer for further film growth [4–8], with deposition on Si being often required. As the typical deposition temperature for high-quality crystalline AlN is usually in excess of 800 °C [9,10], there is a large amount of thermal strain in the films and it is advantageous to develop processes to lower the deposition temperature so that it is compatible with back end of line (BEOL) processing. Plasma enhanced atomic layer deposition (PEALD) of AlN has been extensively studied as a potential solution [11–18]; however, this process relies on a reactive nitrogen-containing plasma (N_2 or NH_3) which can affect the stoichiometry of the deposited films and imposes a limit to the tunability of ion energy/momentum, which is key to depositing large grain crystalline films [19–23].

In this work, the low-temperature (≤400 °C) deposition of polycrystalline AlN films on Si(111) is demonstrated by atomic layer annealing (ALA) which is a variant of atomic layer deposition (ALD) that utilizes a third pulse of low-energy inert gas ions in addition to the usual metal and co-reactant pulses (See Fig. 1) [24]. Using this technique, the stoichiometries of the films are determined by the thermal reaction of the metal and co-reactant while the crystallinity is controlled by the plasma treatment with a non-reactive gas.

Using trimethyl aluminum (TMA) or tris(dimethylamido) aluminum (TDMAA) with the highly-reactive nitrogen-containing precursor hydrazine (N_2H_4), AlN can be deposited at ~200 °C [25,26]; however, these films are amorphous. Using TDMAA with N_2H_4 or NH_3 at temperatures ≥350 °C, polycrystalline films can be deposited in a purely thermal process; however, the reported grain sizes are small (<5 nm) or there is a mixture of polycrystalline and amorphous phases [27,28]. ALA has been used to deposit crystalline films such as AlN [24,29] and GaN [30] on a near lattice-matched substrate (sapphire) at low temperatures, but a N_2/H_2 plasma was used and the effects of substrate biasing were not explored.

In the present study of ALA AlN on Si(111) (a non-lattice matched substrate), two metal precursors (TMA and TDMAA) were compared using ultra-high purity anhydrous N_2H_4 as a co-reactant and argon ions with tuned energy for the third pulse. It was found that ALA deposition using TDMAA as the Al precursor resulted in high-quality AlN films with

* Corresponding author.
E-mail address: akummel@ucsd.edu (A.C. Kummel).

https://doi.org/10.1016/j.apsusc.2021.149656
Received 20 December 2020; Received in revised form 23 February 2021; Accepted 23 March 2021
Available online 26 March 2021
0169-4332/© 2021 Published by Elsevier B.V.

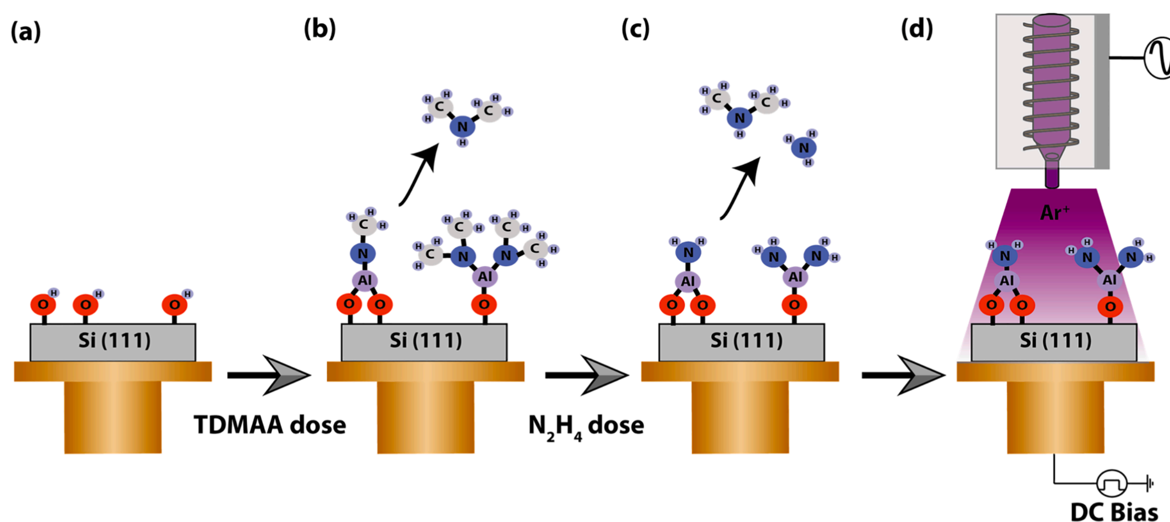

Fig. 1. Schematic Diagram of ALA AlN. (a) Beginning with a hydroxyl-terminated Si wafer, (b) TDMAA is introduced leaving the surface terminated in aluminum dimethylamide. (c) Introduction of N_2H_4 removes the surface bound dimethylamide as dimethylamine gas. (d) The final step in the ALA process consists of low-energy ion bombardment which helps to induce surface mobility and crystalize the film. This 3-step process can be repeated any number of times to achieve the desired thickness.

large grain size (>9 nm) and low C/O contamination (<2 at. %) whereas films deposited using TMA had much higher carbon content (>5 at. %), owing to its thermal instability at 400 °C [31–33]. Transmission electron micrographs for a 10 nm ALA AlN film grown using TDMAA and N_2H_4 show vertical grain structure with grains spanning the entire thickness of the film. As heat spreading layers often need to be in excess of 250 nm thick in order to be relevant for use in high volume manufacturing, it was also demonstrated that ALA-deposited films successfully enhance the grain size of a thick sputtered AlN film by acting as a template layer.

2. Methods

Materials. Si(1 1 1) substrate wafers (phosphorous doped, n-type) with a resistivity of 1–20 ohm-cm were purchased from Waferworld. Acetone (99.5+%), methanol (99.5+%), and deionized (DI) water (99.5%+) were purchased from Fisher Scientific. Hydrofluoric (HF) acid (48%) was purchased from VWR and diluted down to 2% with DI water before use. Ar (99.999%) was purchased from Praxair and purified using an Entegris Gatekeeper gas purifier before being used as both the plasma gas as well as the precursor carrier gas. TMA (98+%) was purchased from Strem chemicals. Ammonia (99.999%) was purchased from Praxair. TDMAA was supplied by EMD performance materials. BRUTE anhydrous hydrazine (30 ppb vapor phase H_2O) was supplied by RASIRC.

Sample preparation. Si samples were first degreased using 10 s rinses in acetone, methanol, and DI water. Following the degrease, native oxides were removed via a cyclic HF clean consisting of 1 min immersions in HF and DI water for 2.5 cycles. Immediately following the clean, the samples were loaded onto a sample holder and pumped down to a pressure of $<2 \times 10^{-6}$ Torr before loading into the deposition chamber.

AlN deposition. The ALA deposition was conducted in a home-built chamber (wall temp = 90 °C) with a base pressure $<1 \times 10^{-6}$ Torr and consisted of a home-built reactor pumped by a dry pump (Edwards EPX 500NE) protected by a liquid nitrogen cold trap and stainless steel mesh particle trap (See Fig. S1). The stage allows for sample biasing and consists of an electrically isolated copper block heated by a cartridge heater. Dosing was performed using pneumatically actuated diaphragm valves and although self-saturating behavior was not observed, pulse times were optimized for growth rates of ~0.9 Å/cycle in order to keep the film thickness between each ALA treatment constant. TDMAA was dosed using a bottle temperature of 105 °C while all other precursors were kept at room temperature. TMA was dosed under its own vapor pressure while both the TDMAA and N_2H_4 cylinders were charged with Ar carrier gas in order to deliver the precursors to the sample. For larger exposures, multiple doses of TDMAA and N_2H_4 were used in order to recharge the cylinders with Ar carrier gas and deliver the precursors. As TMA has sufficient vapor pressure, this technique was not needed and longer pulse times could be used. Gas flows were controlled by mass flow controllers and fed into a RF remote plasma source (PIE Scientific) with a quartz plasma tube mounted above the chamber. ALA used a 20 s plasma treatment each cycle using Ar gas at a pressure of 5 mTorr at a power of 75 W with a pulsed stage bias of −25 VDC (See bias optimization, Fig S2 a-b). For bilayer samples (ALA AlN + sputtered AlN), following ALA deposition, samples were transported *in vacuo* to an attached sputter chamber (base pressure $\sim 2 \times 10^{-6}$ Torr) where AlN was deposited using a Torus Magkeeper sputter cathode (Kurt Lesker) using a 2 in. diameter Al target and 100% N_2 gas at a pressure of 3 mTorr and 300 W of RF power. Amorphous AlN layers were deposited under similar sputtering conditions but at a pressure of 30 mTorr.

X-ray photoelectron spectroscopy (XPS). Samples were transferred from the deposition chamber to the UHV analysis (Omicron VT, base pressure 5×10^{-10} Torr) chamber *in vacuo*. High resolution XP spectra were acquired on the as-deposited samples without any surface treatment (e.g., Ar sputtering or UHV annealing) using a Mg Kα source ($h\nu$ = 1253.6 eV) and DESA 150 electron analyzer (Staib Instruments) at a collection angle of 45° relative to the surface normal using a step width of 0.1 eV. Analysis of the XPS data was performed in CasaXPS v2.3 using Shirley background subtraction and Scofield photoionization cross sectional relative sensitivity factors.

Structural Analysis. Ex situ grazing incidence x-ray diffractometry (GIXRD) and X-ray reflectometry (XRR) were carried out on a diffractometer (Smartlab, Rigaku) using a Cu Kα source (λ = 0.154 nm) operating at 40 kV. Simulation and fitting of the XRR data was carried out using the Smartlab Studio software suite (Rigaku). Cross-sectional transmission electron microscopy (TEM) was used to evaluate the fine grain structure of the deposited films and was performed at Applied Materials.

3. Results and discussion

Two Al precursors (TMA and TDMAA) were first benchmarked at 225 °C. Using a purely thermal process, sequential doses of either 400

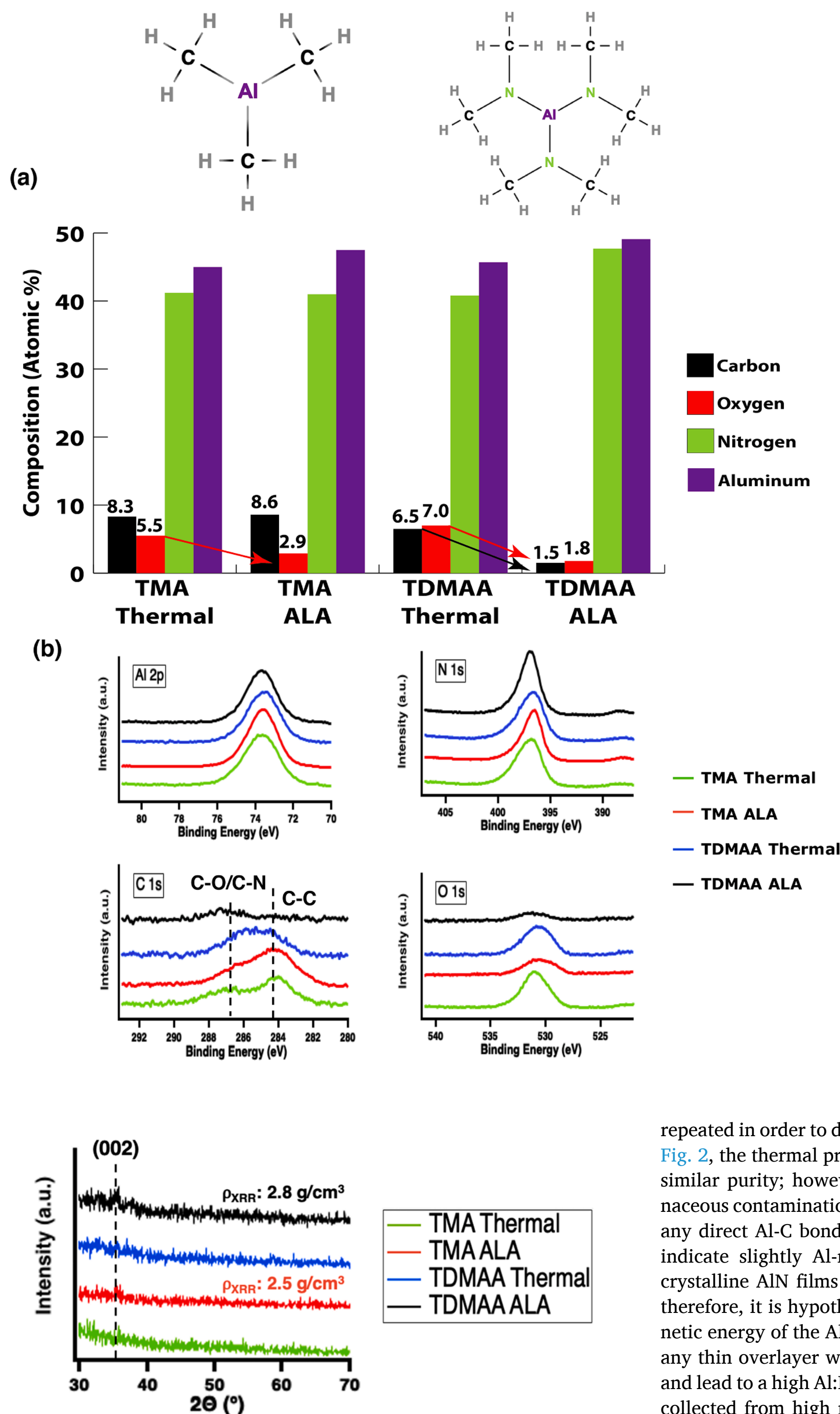

Fig. 2. XPS Chemical Composition Data for both Thermal and ALA Processes using TMA and TDMAA at 225 °C. (a) The chemical compositions for the thermal process using TMA or TDMAA are very similar, with the ALA process resulting in the removal of unwanted C/O, especially when using TDMAA. Molecular schematics of the two precursors are shown (as monomers) above the corresponding XPS data. (b) High resolution XP spectra show chemical shift consistent with stochiometric AlN formation and the effect of ALA on the C/O contamination.

Fig. 3. XRD Data for both Thermal and ALA Processes using TMA and TDMAA at 225 °C. The deposited films are either amorphous or nanocrystalline. Note that even when small crystalline peaks are observed for the ALA process, density via XRR is much lower than bulk crystalline AlN.

ms TMA and 2 × 100 ms pulses of N_2H_4 with 5 s purge times or 2 × 300 ms TDMAA with a 4 s purge and 100 ms N_2H_4 with an 8 s purge were used. For ALA samples, each cycle also included a 20 s Ar plasma treatment with the stage biased at −25 VDC. This cyclic process was repeated in order to deposit films ~40 nm in thickness. As can be seen in Fig. 2, the thermal process for both TDMAA and TMA results in films of similar purity; however, the ALA process removes much more carbonaceous contamination in the case of TDMAA, possibly due to the lack of any direct Al-C bonding in TDMAA. Although the XPS data appear to indicate slightly Al-rich films, it is noted that spectra collected on crystalline AlN films also have Al:N ratios ranging from ~1.05–1.1:1; therefore, it is hypothesized that this artifact arises from the higher kinetic energy of the Al 2p electrons as compared to the N 1s electrons as any thin overlayer would lead to higher attenuation of the N 1s signal and lead to a high Al:N ratio when measured by XPS. Chemical shift data collected from high resolution XP spectra are consistent with the formation of stoichiometric AlN and also demonstrate the beneficial effect of ALA on C/O contamination in these films.

Structural analysis of these films via XRD show that all samples had at best marginal crystallinity regardless of process (Fig. 3). Though small XRD peaks corresponding to AlN (002) were observed for the ALA process, the density of these films as measured by XRR was found to be 2.5 and 2.8 g/cm^3 for the TMA ALA and TDMAA ALA sample, respectively, which is >15% lower than the bulk value for crystalline AlN and likely indicates large percentages of the films are amorphous. Previous studies on PEALD deposited AlN using low (<100 W) power also note

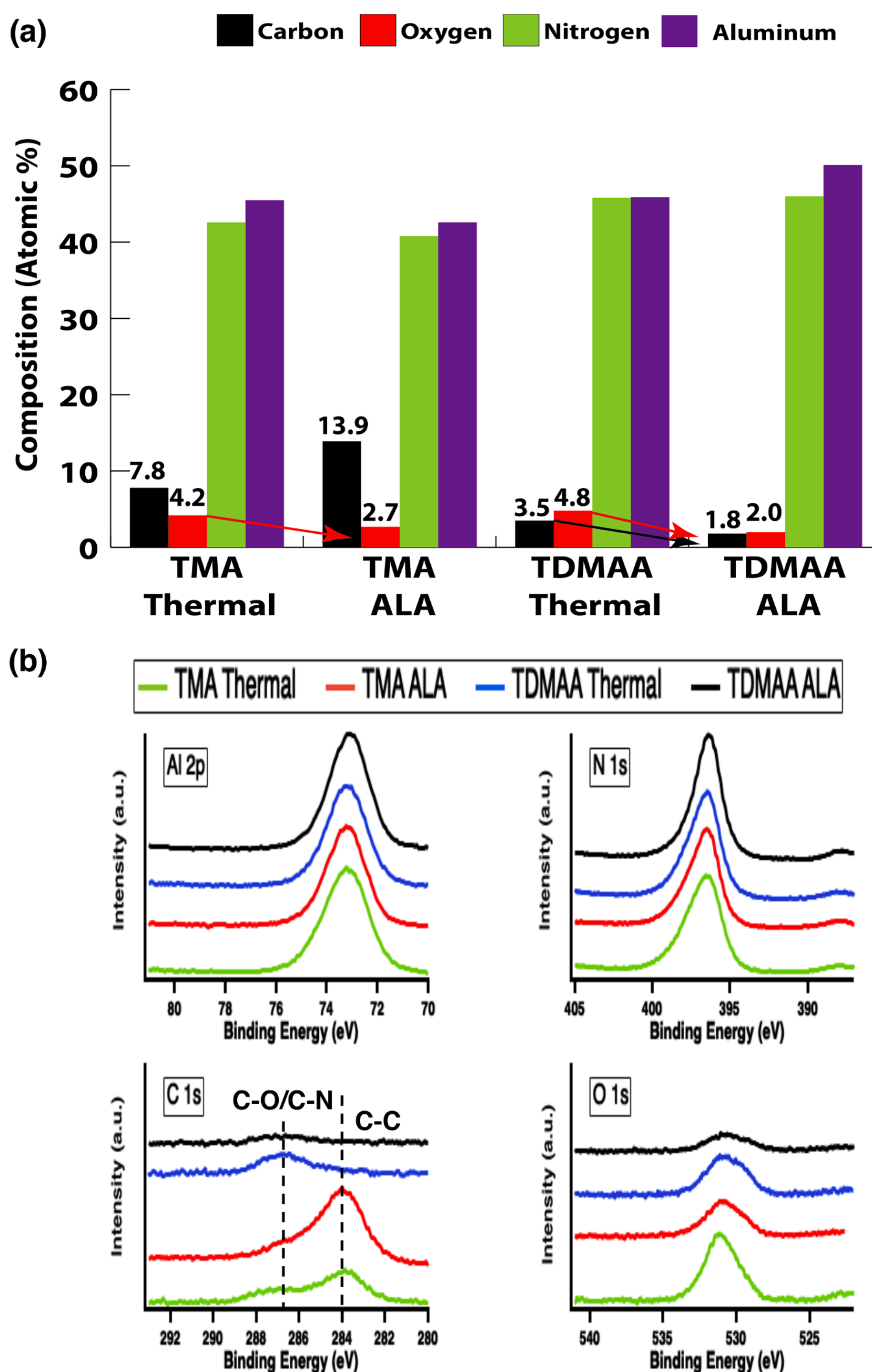

Fig. 4. XPS Chemical Composition Data for both Thermal and ALA Processes using TMA and TDMAA at 400 °C. (a) At 400 °C substrate temperature, films grown using TDMAA have lower impurity content, with the ALA films containing the lowest impurity content of <2 at. % C/O. (b) High resolution XP spectra show chemical shift consistent with stoichiometric AlN formation and the effect of ALA on the C/O contamination.

that at lower temperatures, crystallization of the film does not occur at T < 300 °C [17] and that either higher deposition temperature or increased plasma power were needed to form crystalline films [15,34,35], with these results being in rough agreement with the work of Bosund et al. [17] after taking into account these thinner films of ~40 nm will display poorer crystallinity due to higher dislocation density close to the interface.

Since thermal AlN films are typically seen to crystallize at temperatures of 350–375 °C, the same two precursors were compared at 400 °C deposition temperature to elucidate the impact of the ALA process on weakly crystalline films. As all temperatures at which thermal crystallization of AlN would occur are higher than the decomposition temperature of TMA [31–33,36,37], the highest temperature allowed for BEOL processing (~400 °C) was chosen. Owing to the improved reactivities of the precursors at 400 °C, precursor pulses were modified to 35 ms TMA with a 10 s purge and 100 ms N_2H_4 with an 8 s purge or 150 ms TDMAA with a 4 s purge and 100 ms N_2H_4 with an 8 s purge. ALA samples received the same 20 s Ar plasma treatment with the stage biased at −25 VDC used previously. Due to the thermal decomposition of TMA at 400 °C, the lowest growth rate attainable was 1.8 Å/cycle. As it

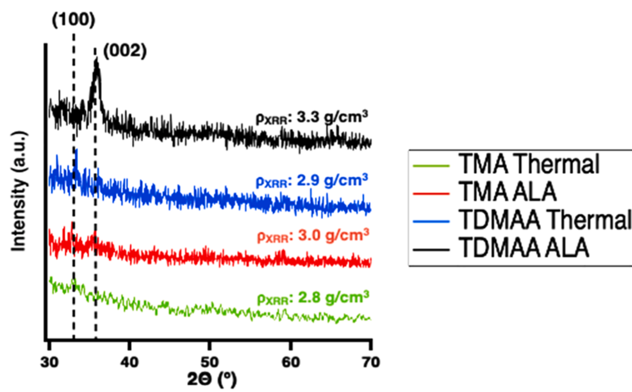

Fig. 5. XRD Data for both Thermal and ALA Processes using TMA and TDMAA at 400 °C. Films grown using TDMAA ALA display oriented (0 0 2) growth as compared to the other processes which are predominantly (1 0 0) oriented, mixed phase, or amorphous. Note bulk-like AlN density is only achieved for TDMAA ALA.

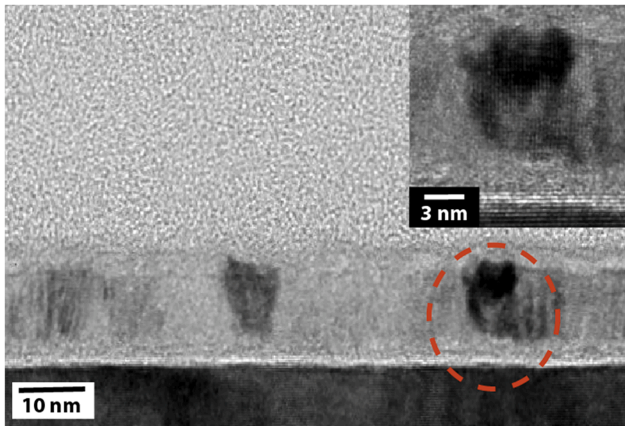

Fig. 6. Bright Field TEM Image of a 10 nm ALA AlN layer. Template layers are smooth by TEM and have large grains that extend through the entire thickness of the film (inset: high resolution TEM showing the lattice fringes).

can be seen in Fig. 4, films grown using TDMAA have lower impurity concentration for both the thermal as well as ALA processes and the ALA TDMAA process has lower impurities than the thermal ALD TDMAA process. Although the precise mechanism for the reduction in impurity content from ALA is not known, it is hypothesized that this effect is due to either a gentle sputtering process that removes surface oxides and carbonaceous species (including unreacted ligands) or that the enhanced density as a result of the ALA prevents the incorporation of these impurities into the film. It is noted that at 400 °C using TMA, the ALA process increases the carbon content in the AlN films. This is likely linked to the thermal instability of TMA at high temperatures which may result in the generation of carbon-containing species such as gaseous methyl radicals that the plasma then imbeds in the AlN films. In contrast, because TDMAA does not contain any C-Al bonds and has high thermally stability at 400 °C, the resulting AlN films do not contain high levels of carbon [38,39]. NH_3 was tested as an alternative co-reactant for the ALA process at 400 °C; however, owing to the lower reactivity as compared to N_2H_4, growth rate was reduced and O contamination was increased (Fig S3). From the high-resolution carbon XP spectra (Fig. 4b), it is seen that for the TDMAA ALA process, aliphatic carbon is reduced to below detection limits while the remaining component just above detection limits is likely surface bound dimethylamide. Especially noteworthy is the ALA process with TDMAA achieves extremely low impurity concentration (<2 at. % C/O) even without sputtering into the bulk of the film.

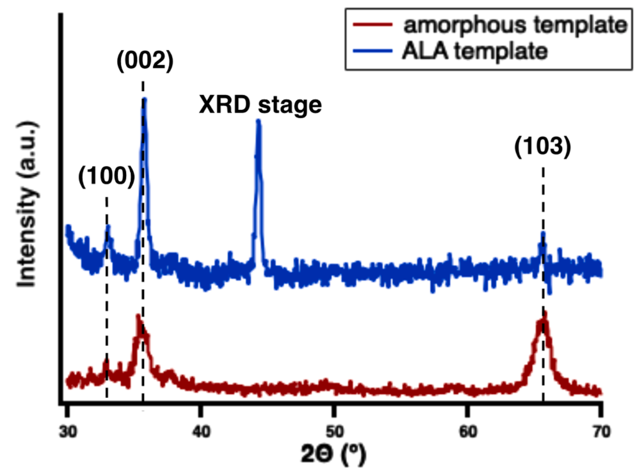

Fig. 7. XRD data comparing AlN films using a 25 nm amorphous AlN buffer layer with a 25 nm ALA AlN buffer layer. Replacing the amorphous AlN buffer layer with ALA AlN results in a >2x improvement in grain size for equivalent thickness of sputtered material.

Subsequent XRD analysis (Fig. 5) confirms that the TDMAA ALA process leads to the highest quality films of oriented c-axis AlN. The film densities of the ALA samples were measured by XRR to be 3.0 g/cm^3 and 3.3 g/cm^3 for the TMA ALA and TDMAA sample, respectively, which indicates that the elevated carbon content in the TMA ALA sample likely prevented crystallization while the TDMAA ALA sample has a density within 1% of bulk crystalline AlN and a full width at half the maximum intensity (FWHM) value of 0.95°, which corresponds to a crystallite size of ~9.2 nm by the Scherer equation [40].

In order to demonstrate the effect of these ALA-deposited layers, sputter deposition was identified as one method capable of quickly depositing crystalline AlN at temperatures compatible with BEOL processing. Sputter-deposited AlN films can contain large amounts of compressive strain [41] when deposited on Si(1 1 1) and so it is necessary to use a buffer layer in order to avoid cracking or flaking of the deposited film. Thin, 25 nm ALA AlN films grown using TDMAA were subsequently deposited for use as templates for the growth of 290 nm of sputter deposited AlN and compared against a buffer layer composed of 25 nm of amorphous AlN. As it can be seen in Fig. 6, the template layers deposited via ALA on a non-lattice-matched substrate Si(1 1 1) are smooth and contain grains >10 nm wide that span the entire thickness of the film.

The initial growth stages of sputtering are an essentially stochastic process when performed on a non-lattice matched substrate. This results in multiple grain orientations or the formation of dislocations/defects that reduce the average grain size of the sputtered material. Due to the ALA template acting as a lattice matched substrate, it was expected that sputtered films grown on the ALA layers would have larger average grain size with and have stronger (0 0 2) preferential orientation as compared to the amorphous AlN buffer layers. As it can be seen in Fig. 7, XRD data show that sputtered AlN grown on amorphous AlN is polycrystalline (0 0 2)/(1 0 3) with no preferential orientation while the AlN grown on the ALA AlN template is highly textured (0 0 2). TEM data of the sample grown on ALA AlN (Fig. 8) show the grain structure of the sputtered layer originating from the ALA layer which then serves to template the columnar growth of the film. When comparing the FWHM of the (0 0 2) peak, the sample grown on amorphous AlN has a much larger FWHM (1.09°) as compared to the sample grown on ALA AlN (0.45°) which corresponds to an increase in average grain size from 8 nm to 19.4 nm by using the ALA template layer.

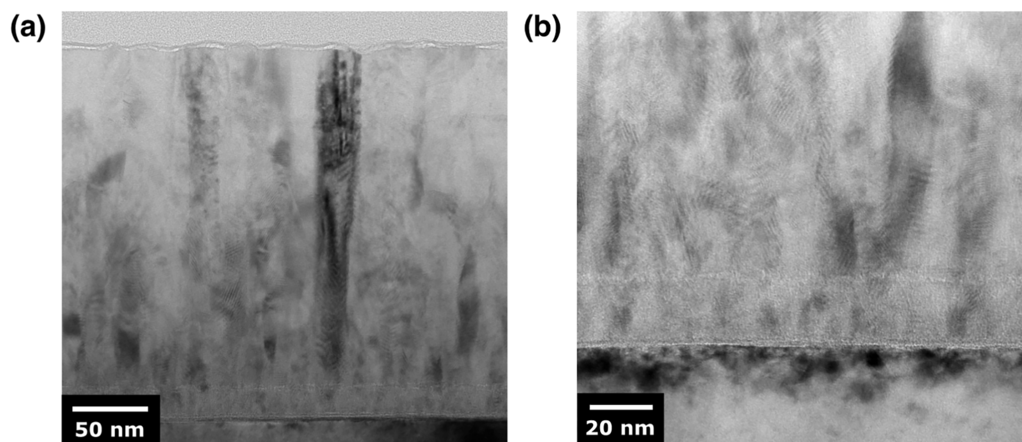

Fig. 8. Bright Field TEM Image of a 25 nm ALA AlN templating the growth of 290 nm sputtered AlN. (a) Columnar grains are observed that extend from the top of the film to the substrate. (b) The sputtered grain structure originates from the template layer and then grows vertically.

4. Conclusion

In summary, it is demonstrated that precursor selection is key for developing processes for the low-temperature deposition of oriented crystalline materials on non-lattice matched substrates such as Si(1 1 1). It is shown that even at the relatively modest temperature of 400 °C, commonly used precursors such as TMA do not possess the thermal stability needed in order to deposit high quality crystalline films and that there exists a need for non-intuitive precursors such as TDMAA and N_2H_4. Through the selection of precursors that are thermally stable, yet highly reactive, oriented c-axis AlN films are able to be grown on Si via bias enhanced ALA. These films have an average grain size >9 nm and are successfully shown to template the growth of sputtered AlN which results in a >2x increase in the average grain size (19 nm) as compared to an AlN film sputtered on amorphous AlN (8 nm). As this process does not require a lattice-matched substrate and is BEOL compatible, it is relevant for a wide range of applications ranging from buffer layer deposition to CMOS/RF heat spreaders.

Declaration of Competing Interest

The authors declare that they have no known competing financial interests or personal relationships that could have appeared to influence the work reported in this paper.

Acknowledgement

This work was supported in part by the Applications and Systems-Driven Center for Energy Efficient Integrated Nano Technologies (ASCENT), one of six centers in the Joint University Microelectronics Program (JUMP), an SRC program sponsored by the Defense Advanced Research Program Agency (DARPA). The authors would also like to gratefully acknowledge support from Applied Materials, RASIRC, and EMD.

Author credit statement

S.T.U. and A.M. performed the sample deposition, assisted with all data analysis, and wrote the manuscript with contributions from all authors. D.A. provided technical expertise on the installation and use of the anhydrous N_2H_4 source. R.K., M.M., and J.W. provided key expertise on the synthesis, purification, and use of the TDMAA precursor. A.C.K. directed the study and assisted with all data analysis.

Appendix A. Supplementary data

Supplementary data to this article can be found online at https://doi.org/10.1016/j.apsusc.2021.149656.

References

[1] R.L. Xu, M. Munõz Rojo, S.M. Islam, A. Sood, B. Vareskic, A. Katre, N. Mingo, K. E. Goodson, H.G. Xing, D. Jena, et al., Thermal Conductivity of Crystalline AlN and the Influence of Atomic-Scale Defects, J. Appl. Phys. (2019), https://doi.org/10.1063/1.5097172.

[2] Y.J. Heo, H.T. Kim, K.J. Kim, S. Nahm, Y.J. Yoon, J. Kim, Enhanced Heat Transfer by Room Temperature Deposition of AlN Film on Aluminum for a Light Emitting Diode Package, Appl. Therm. Eng. (2013), https://doi.org/10.1016/j.applthermaleng.2012.07.024.

[3] L. La Spina, E. Iborra, H. Schellevis, M. Clement, J. Olivares, L.K. Nanver, Aluminum Nitride for Heatspreading in RF IC's, Solid. State. Electron. (2008), https://doi.org/10.1016/j.sse.2008.04.009.

[4] H. Lu, W.J. Schaff, J. Hwang, H. Wu, G. Koley, L.F. Eastman, Effect of an AlN Buffer Layer on the Epitaxial Growth of InN by Molecular-Beam Epitaxy, Appl. Phys. Lett. (2001), https://doi.org/10.1063/1.1402649.

[5] F.A. Ponce, J.S. Major, W.E. Plano, D.F. Welch, Crystalline Structure of AlGaN Epitaxy on Sapphire Using AlN Buffer Layers, Appl. Phys. Lett. (1994), https://doi.org/10.1063/1.112724.

[6] H. Amano, I. Akasaki, K. Hiramatsu, N. Koide, N. Sawaki, Effects of the Buffer Layer in Metalorganic Vapour Phase Epitaxy of GaN on Sapphire Substrate, Thin Solid Films (1988), https://doi.org/10.1016/0040-6090(88)90458-0.

[7] J.N. Kuznia, M.A. Khan, D.T. Olson, R. Kaplan, J. Freitas, Influence of Buffer Layers on the Deposition of High Quality Single Crystal GaN over Sapphire Substrates, J. Appl. Phys. (1993), https://doi.org/10.1063/1.354069.

[8] T. Shiino, S. Shiba, N. Sakai, T. Yamakura, L. Jiang, Y. Uzawa, H. Maezawa, S. Yamamoto, Improvement of the Critical Temperature of Superconducting NbTiN and NbN Thin Films Using the AlN Buffer Layer, Supercond. Sci. Technol. (2010), https://doi.org/10.1088/0953-2048/23/4/045004.

[9] Y. Chen, H. Song, D. Li, X. Sun, H. Jiang, Z. Li, G. Miao, Z. Zhang, Y. Zhou, Influence of the Growth Temperature of AlN Nucleation Layer on AlN Template Grown by High-Temperature MOCVD, Mater. Lett. (2014), https://doi.org/10.1016/j.matlet.2013.09.096.

[10] A. Kakanakova-Georgieva, D. Nilsson, E. Janzén, High-Quality AlN Layers Grown by Hot-Wall MOCVD at Reduced Temperatures, J. Cryst. Growth (2012), https://doi.org/10.1016/j.jcrysgro.2011.10.052.

[11] H. Van Bui, F.B. Wiggers, A. Gupta, M.D. Nguyen, A.A.I. Aarnink, M.P. de Jong, A. Y. Kovalgin, Initial Growth, Refractive Index, and Crystallinity of Thermal and Plasma-Enhanced Atomic Layer Deposition AlN Films, J. Vac. Sci. Technol. A Vacuum, Surf., Film. (2015), https://doi.org/10.1116/1.4898434.

[12] P. Sippola, A. Pyymaki Perros, O.M.E. Ylivaara, H. Ronkainen, J. Julin, X. Liu, T. Sajavaara, J. Etula, H. Lipsanen, R.L. Puurunen, Comparison of Mechanical Properties and Composition of Magnetron Sputter and Plasma Enhanced Atomic Layer Deposition Aluminum Nitride Films, J. Vac. Sci. Technol. A (2018), https://doi.org/10.1116/1.5038856.

[13] S.; Aarnink, A.A.I. van de Kruijs, R. Kovalgin, A.Y. Schmitz, J. PEALD AlN: Controlling Growth and Film Crystallinity. Phys. Status Solidi Curr. Top. Solid State Phys. 2015. https://doi.org/10.1002/pssc.201510039.

[14] M. Alevli, C. Ozgit, I. Donmez, N. Biyikli, Structural Properties of AlN Films Deposited by Plasma-Enhanced Atomic Layer Deposition at Different Growth Temperatures, Phys. Status Solidi Appl. Mater. Sci. (2012), https://doi.org/10.1002/pssa.201127430.

[15] V. Tarala, M. Ambartsumov, A. Altakhov, V. Martens, M. Shevchenko, Growing C-Axis Oriented Aluminum Nitride Films by Plasma-Enhanced Atomic Layer Deposition at Low Temperatures, J. Cryst. Growth (2016), https://doi.org/10.1016/j.jcrysgro.2016.10.015.
[16] P. Motamedi, K. Cadien, Structural and Optical Characterization of Low-Temperature ALD Crystalline AlN, J. Cryst. Growth (2015), https://doi.org/10.1016/j.jcrysgro.2015.04.009.
[17] M. Bosund, T. Sajavaara, M. Laitinen, T. Huhtio, M. Putkonen, V.M. Airaksinen, H. Lipsanen, Properties of AlN Grown by Plasma Enhanced Atomic Layer Deposition, Appl. Surf. Sci. (2011), https://doi.org/10.1016/j.apsusc.2011.04.037.
[18] S. Liu, M. Peng, C. Hou, Y. He, M. Li, X. Zheng, PEALD-Grown Crystalline AlN Films on Si (100) with Sharp Interface and Good Uniformity, Nanoscale Res. Lett. (2017), https://doi.org/10.1186/s11671-017-2049-1.
[19] J. Wang, R.L. Maier, H. Schreiber, Crystal Phase Transition of HfO2 Films Evaporated by Plasma-Ion-Assisted Deposition, Appl. Opt. (2008), https://doi.org/10.1364/AO.47.00C189.
[20] J.-S. Park, H.-S. Park, S.-W. Kang, Plasma-Enhanced Atomic Layer Deposition of Ta-N Thin Films, J. Electrochem. Soc. (2002), https://doi.org/10.1149/1.1423642.
[21] H.B. Profijt, M.C.M. Van De Sanden, W.M.M. Kessels, Substrate Biasing during Plasma-Assisted ALD for Crystalline Phase-Control of TiO 2 Thin Films, Electrochem. Solid-State Lett. (2012), https://doi.org/10.1149/2.024202esl.
[22] H.B. Profijt, M.C.M. van de Sanden, W.M.M. Kessels, Substrate-Biasing during Plasma-Assisted Atomic Layer Deposition to Tailor Metal-Oxide Thin Film Growth, J. Vac. Sci. Technol. A Vacuum, Surf., Film. (2013), https://doi.org/10.1116/1.4756906.
[23] T. Faraz, H.C.M. Knoops, M.A. Verheijen, C.A.A. Van Helvoirt, S. Karwal, A. Sharma, V. Beladiya, A. Szeghalmi, D.M. Hausmann, J. Henri, et al., Tuning Material Properties of Oxides and Nitrides by Substrate Biasing during Plasma-Enhanced Atomic Layer Deposition on Planar and 3D Substrate Topographies, ACS Appl. Mater. Interfaces (2018), https://doi.org/10.1021/acsami.8b00183.
[24] H.Y. Shih, W.H. Lee, W.C. Kao, Y.C. Chuang, R.M. Lin, H.C. Lin, M. Shiojiri, M. J. Chen, Low-Temperature Atomic Layer Epitaxy of AlN Ultrathin Films by Layer-by-Layer, in-Situ Atomic Layer Annealing, Sci. Rep. (2017), https://doi.org/10.1038/srep39717.
[25] M. Mizuta, S. Fujieda, Y. Matsumoto, T. Kawamura, Low Temperature Growth of Gan and Ain on Gaas Utilizing Metalorganics and Hydrazine, Jpn. J. Appl. Phys. (1986), https://doi.org/10.1143/JJAP.25.L945.
[26] Y.C. Jung, S.M. Hwang, D.N. Le, A.L.N. Kondusamy, J. Mohan, S.W. Kim, J.H. Kim, A.T. Lucero, A. Ravichandran, H.S. Kim, et al., Low Temperature Thermal Atomic Layer Deposition of Aluminum Nitride Using Hydrazine as the Nitrogen Source, Materials (Basel). (2020), https://doi.org/10.3390/ma13153387.
[27] R.G. Gordon, U. Riaz, D.M. Hoffman, Chemical Vapor Deposition of Aluminum Nitride Thin Films, J. Mater. Res. 7 (7) (1992) 1679–1684, https://doi.org/10.1557/JMR.1992.1679.
[28] A.I. Abdulagatov, S.M. Ramazanov, R.S. Dallaev, E.K. Murliev, D.K. Palchaev, M. K. Rabadanov, I.M. Abdulagatov, Atomic Layer Deposition of Aluminum Nitride Using Tris(Diethylamido)Aluminum and Hydrazine or Ammonia, Russ. Microelectron. (2018), https://doi.org/10.1134/S1063739718020026.
[29] W.C. Kao, W.H. Lee, S.H. Yi, T.H. Shen, H.C. Lin, M.J. Chen, AlN Epitaxy on SiC by Low-Temperature Atomic Layer Deposition: Via Layer-by-Layer, in Situ Atomic Layer Annealing, RSC Adv. (2019), https://doi.org/10.1039/c9ra00008a.
[30] W.H. Lee, Y.T. Yin, P.H. Cheng, J.J. Shyue, M. Shiojiri, H.C. Lin, M.J. Chen, Nanoscale GaN Epilayer Grown by Atomic Layer Annealing and Epitaxy at Low Temperature, ACS Sustain. Chem. Eng. (2019), https://doi.org/10.1021/acssuschemeng.8b03982.
[31] S. Yamashita, K. Watanuki, H. Ishii, Y. Shiba, M. Kitano, Y. Shirai, S. Sugawa, T. Ohmi, Dependence of the Decomposition of Trimethylaluminum on Oxygen Concentration, J. Electrochem. Soc. (2011), https://doi.org/10.1149/1.3517080.
[32] D. Riihelä, M. Ritala, R. Matero, M. Leskelä, J. Jokinen, P. Haussalo, Low Temperature Deposition of AlN Films by an Alternate Supply of Trimethyl Aluminum and Ammonia, Chem. Vap. Depos. (1996), https://doi.org/10.1002/cvde.19960020612.
[33] P. Rouf, P. Sukkaew, L. Ojamäe, H. Pedersen, Reduction of Carbon Impurities in Aluminum Nitride from Time-Resolved Chemical Vapor Deposition Using Trimethylaluminum, J. Phys. Chem. C (2020), https://doi.org/10.1021/acs.jpcc.0c01724.
[34] C. Ozgit, I. Donmez, M. Alevli, N. Biyikli, Self-Limiting Low-Temperature Growth of Crystalline AlN Thin Films by Plasma-Enhanced Atomic Layer Deposition, Thin Solid Films (2012), https://doi.org/10.1016/j.tsf.2011.11.081.
[35] C. Ozgit-Akgun, E. Goldenberg, A.K. Okyay, N. Biyikli, Hollow Cathode Plasma-Assisted Atomic Layer Deposition of Crystalline AlN, GaN and AlxGa1-XN Thin Films at Low Temperatures, J. Mater. Chem. C (2014), https://doi.org/10.1039/c3tc32418d.
[36] D.W. Squire, Mechanistic Studies of the Decomposition of Trimethylaluminum on Heated Surfaces, J. Vac. Sci. Technol. B Microelectron. Nanom. Struct. (1985), https://doi.org/10.1116/1.582976.
[37] T.R. Gow, R. Lin, L.A. Cadwell, F. Lee, A.L. Backman, R.I. Masel, Decomposition of Trimethylaluminum on Si(100), Chem. Mater. (1989), https://doi.org/10.1021/cm00004a006.
[38] A.I. Abdulagatov, R.R. Amashaev, K.N. Ashurbekova, K.N. Ashurbekova, M.K. Rabadanov, I.M. Abdulagatov, Atomic Layer Deposition of Aluminum Nitride and Oxynitride on Silicon Using Tris(Dimethylamido)Aluminum, Ammonia, and Water, Russ. J. Gen. Chem. (2018). https://doi.org/10.1134/S1070363218080236.
[39] S.C. Buttera, D.J. Mandia, S.T. Barry, Tris(Dimethylamido)Aluminum(III): An Overlooked Atomic Layer Deposition Precursor. J. Vac. Sci. Technol. A Vacuum, Surfaces, Film. 2017. https://doi.org/10.1116/1.4972469.
[40] P. Scherrer, Bestimmung Der Größe Und Der Inneren Struktur von Kolloidteilchen Mittels Röntgenstrahlen, Math. Klasse, Nachrichten von der Gesellschaft der Wissenschaften zu Göttingen, 1918.
[41] K. Kusaka, D. Taniguchi, T. Hanabusa, K. Tominaga, Effect of Sputtering Gas Pressure and Nitrogen Concentration on Crystal Orientation and Residual Stress in Sputtered AlN Films, Vacuum (2002), https://doi.org/10.1016/S0042-207X(02)00168-9.